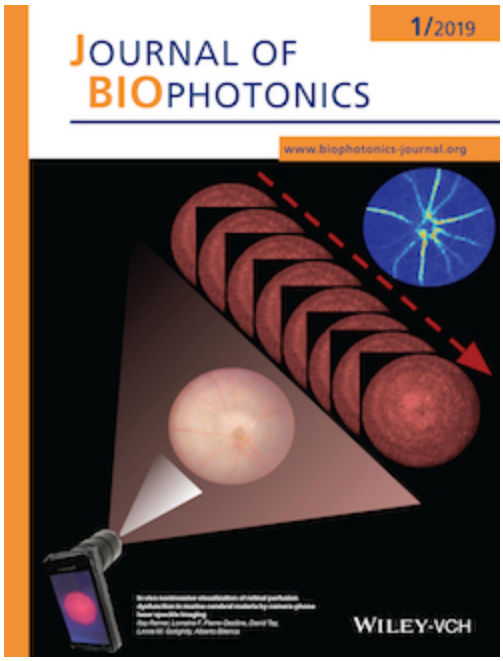

Method for stereotactic biopsy guidance based on analysis of OCT images in two polarization channels

Journal:	*Journal of Biophotonics*
Manuscript ID	Draft
Wiley - Manuscript type:	Full Article
Date Submitted by the Author:	n/a
Complete List of Authors:	Moiseev, Alexander; Institute of Applied Physics RAS,
Keywords:	

Method for stereotactic biopsy guidance based on analysis of OCT images in two polarization channels

Alexander A. Moiseev[*,1], *Elena B. Kiseleva*[2], *Konstantin S. Yashin*[2], *Sergey S. Kuznetsov*[2], *Grigory V. Gelikonov*[1], *Igor. A. Medyanik*[2], *Leonid Ya. Kravets*[2], *Elena V. Zagaynova*[2], *Ludmila B. Snopova*[2], *and Natalia D. Gladkova*[2]

[1]Institute of Applied Physics Russian Academy of Sciences, 603950 Ulyanova St., 46, Nizhny Novgorod, Russia
[2] Privolzhskiy Research Medical University, 603950 Minin and Pozharsky Sq., 10/1, Nizhny Novgorod, Russia
* Corresponding author: e-mail: aleksandr.moiseev@gmail.com, Phone: +7 9308000038

Received zzz, revised zzz, accepted zzz
Published online zzz

Key words: Cross-polarization optical coherence tomography (CP OCT), image processing, biopsy guidance

The study aimed to create a machine learning method for differentiating diagnostically valued tumorous tissue from diagnostically "non-valued" non-tumorous tissues in the human brain, using cross-polarization optical coherence tomography (CP OCT) in order to provide guidance for stereotactic biopsies. A method of feature extraction from OCT data in two orthogonal polarization channels has been proposed and a classification algorithm for the resulting feature vectors has been created. If used for stereotactic biopsy guidance, the proposed approach could decrease the number of excised diagnostically non-valued samples and minimize the invasiveness of the procedure and the risk of excessive bleeding.

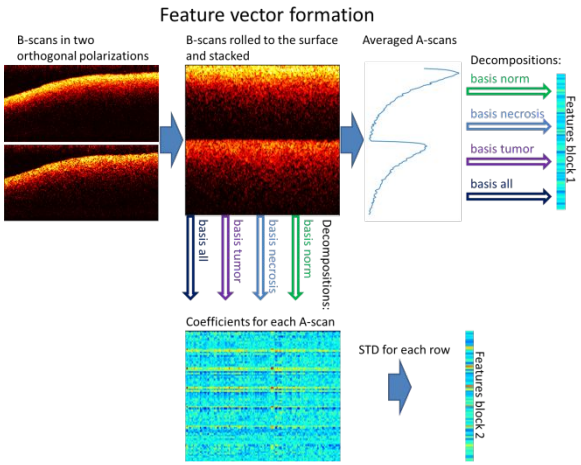

Visualization of feature vector formation process from OCT cross-sectional images in two polarization channels.

1. Introduction

Gliomas are the most common tumors (34 %) of the central nervous system [1, 2], but there has been little progress in the survival rate of the patients despite substantial advances in medical treatment [3, 4]. These kinds of tumor can be characterized by aggressive infiltrative growth into the surrounding brain tissues and thereby the absence of clear boundaries between the cancer and non-cancer tissues, which makes it difficult to distinguish them during surgery in order to minimize the required extent of tumor resection. The introduction of intraoperative fluorescence diagnostics into clinical practice allows a significant enhancement of the ability to identify any remaining tumor, thereby increasing the survival rate [5-9]. Also, clinical testing of fluorescence techniques [10-12] has demonstrated the limitations of using only white light microscopy for achieving total tumor resection, and the requirement for using additional technologies for detecting the "cancer/non-cancer" dividing line.

In the case of wide-spreading gliomas, a stereotactic biopsy to verify the histopathological diagnosis is needed. During this procedure there is a risk of acquisition of non-diagnostic samples from outside the

phys. stat. sol. (a) 201, No. 13 (2004) / www.pss-rapid.com R2

viable tumor volume (such as necrotic/gliotic tissue or normal white matter), a situation that has been reported in up to 24% of stereotactic biopsy series[13-15]. It leads to repeated neurosurgical intervention. Therefore, intratumoral serial biopsies [16, 17] and intraoperative neuropathological assessments [15, 16, 18] are commonly applied to improve the diagnostic yield and accuracy of stereotactic biopsies. These techniques, however, have major drawbacks: (1) intraoperative neuropathological assessment is time-consuming, costly, and not always available [15, 19, 20]; (2) the acquisition of serial biopsies is associated with an increased risk of intracranial hemorrhages; these have been reported in 0.3–59.8% of cases [14, 21, 22] contribute considerably to the reported morbidity up to 16.1% [15, 16, 23, 24] and mortality up to 3.9% [14, 15, 23, 24]. Therefore, the development of a method to determine both the presence of the blood vessels and the presence of tumor tissue in the area of sampling is needed.

Advanced optical bioimaging techniques seem to be the most promising in the furtherance of these goals [25, 26]. One of the best-developed methods for neurological surgical guidance is optical coherence tomography (OCT)[27, 28], which is based on low-coherence interferometry in the near IR range of wavelengths (700–1,300 nm) and allows images of tissue microstructure to be obtained in real-time and with micron resolution at depths of 1–2 mm[29]. This also looks promising for more precise detection of blood vessels. It can be considered as a method of optical biopsy. This method has been using in clinical practice over recent years, particularly in ophthalmology, endovascular surgery, dermatology, and gastroenterology.

A number of *ex vivo* and *in vivo* studies on experimental tumor models, *ex vivo* biopsy specimens and in patients with gliomas have shown good results from OCT, enabling cancer and non-cancer tissue to be distinguished by qualitative (visual) [30, 31] and quantitative[32-34] assessment of the OCT data. Promising preclinical results have stimulated the development of OCT scanning systems for microsurgical guidance, such as OCT handled probes[32, 35] or microscope-integrated OCT[36, 37]. The OCT systems that have been approved provide only a visual assessment of OCT scans, and there is a paucity of studies aimed at defining the visual OCT criteria. Recently we have attempted this for cross-polarization OCT (CP OCT). CP OCT[38, 39] is a variant of polarization-sensitive OCT (PS-OCT) that is based on the birefringence of the medium and provides better visualization of elongated structures – those that have significant longitudinal dimensions (e.g. myelinated nerve fibers). Some advantages of PS-OCT have been shown for the visualization of white matter tracts when compared to the use of traditional OCT[40, 41].

2. Materials and Methods

2.1 OCT setup

The current study was performed with a high-speed OCT device with cross-polarization detection, developed at the Institute of Applied Physics of the Russian Academy of Sciences (Nizhny Novgorod, Russia)[42]. The device operates at a central wavelength of 1.3 μm with axial and lateral resolutions 10 μm and 15 μm in air, respectively. The probing beam has circular polarization. The device uses a 20,000 A-scans/s scanning rate and performs 2D lateral scanning across an area of 2.4x2.4 mm to obtain the 3D distribution of backscattered light in polarizations parallel and orthogonal to the polarization of the probing beam (co- and cross-polarization images, respectively). Scanning was performed in contactless mode.

2.2 Sample acquisition

The *ex vivo* specimens of different tissue types were obtained during tumor resection from 10 patients with gliomas of different degrees of malignancy.

The surgical approach to tumor resection was performed using a frameless navigation system with uploaded functional MRI data and intraoperative neurophysiological monitoring (as well “awake” surgery) for the preservation of the motor and speech eloquent brain areas and white matter tracts. Along the trajectory of the surgical approach, non-tumorous tissue of the peritumoral area, which routinely is subject to coagulation, was accurately marked and removed. Also, during resection of the tumorous tissue, specimens were taken from different parts of the tumor. Each sample was at least 5x5x5 mm. All taken specimens were placed in cotton wool, moistened with saline solution, and sent for OCT scanning within 2 hours. One OCT volume scan was taken from each sample for the present study. After the surgery no deterioration in the condition of the patients compared to the preoperative stage was observed. The study was approved by the Ethical Committee of the Privolzhskiy Federal Research Medical Centre of the Ministry of Health of the Russian Federation, and informed consent of the patients was obtained.

After imaging the specimen, the scanned area was marked with histological ink, then the specimen was fixed in 10% formalin for 48 hours and re-sectioned through the marked area so that the plane of the histological sections coincided *en-face* with the CP OCT images. The histological slides were viewed and photographed with a microscope equipped with a

phys. stat. sol. (a) 201, No. 13 (2004) / www.pss-rapid.com R3

digital camera (Leica DM 2500, DFC 245C) in transmitted light. Two histopathologists independently evaluated the pathological slides stained with H&E. The diagnoses coincided in 98% of cases.
According to the objective of the stereotactic biopsy procedure, and the necessity for obtaining diagnostically valued samples all the obtained tissue samples were classified into two groups: (1) non-tumorous (diagnostically non-valued) tissue including white matter (11 samples), cortex (grey matter) (16 samples) and necrotic tissue (19 samples); (2) tumorous tissue (diagnostically valued) including astrocytoma Grade II-III (28 samples), glioblastoma Grade IV with necrosis (28 samples) and glioblastoma Grade IV without necrosis (16 samples).

2.3 Algorithm for classification of the B-scans

The main goal of the proposed method was to distinguish between samples with tumorous tissue, which can provide viable histological information, and samples, which are of little value for diagnosis (white matter, cortex and areas of necrosis). For that purpose, all the collected samples were divided into three groups: the first one (to train the algorithm), consisted of 5 white matter samples, 7 grey matter samples, 9 necrotic tissue samples, 13 astrocytoma samples, 13 glioblastoma Grade IV with necrosis samples and 7 glioblastoma Grade IV without necrosis samples. The second one, consisted of two samples of each type, in order to validate the algorithm performance and for optimization of the algorithm hyperparameters. The remaining samples were used to test the performance of the resulting algorithm. For each entry, scattering profiles (A-scans) from the surface to a depth of 1 mm were analyzed. The cross-sectional OCT images in both polarization channels were stacked together to form a single vector of 280 values corresponding to the scattering intensity at each of the visualized depths in the initial polarization (first 140 values) and in the orthogonal polarization (last 140 values). Each B-scan was characterized by its averaged scattering profile (A-scan) and the variability of the A-scans across the B-scan. To characterize an individual averaged B-scan, it was decomposed into seven orthogonal sets of functions. Each orthogonal basis was obtained using principal component analysis (PCA) from seven different subsets of the training data: the first from all the available B-scans, the other six from the B-scans of each identified morphological subtype. For dimensionality reduction and to decrease the influence of noise, only the first 8 principal components were retained from each basis, thus each averaged B-scan was characterized using 7x8 = 52 rather than 2x140 = 280 values.

To evaluate the A-scan variability across the B-scan, each A-scan of the B-scan was also decomposed into the same 7 orthogonal sets of 8 vectors each and the variance of every coefficient across the B-scan was used to generate 52 additional values for the classification vector. Thus, each data entry consisting of two B-scans of 256x140 pixels in two polarization channels was represented using 104 values, characterizing he average scattering profile and the scattering profile variability across the B-scans. Based on these 104-features vectors, a random forest classifier was trained that could distinguish all 6 investigated tumor morphology types from each other. A Python Scikit-learn package realization of the Random Forest Classification was used with 100 individual estimators. For each entry, an outcome of the algorithm was six values from 0 to 1, which represent the ranking of the probability of the sample being of a particular morphological type, i.e. the entry is more likely to be of the type with the highest algorithm output. The summation of the three values for the tumor grade provide an overall value for making a decision on whether a biopsy should be taken from the imaged location. A schematic representation of the proposed data processing is presented in Figure 1.

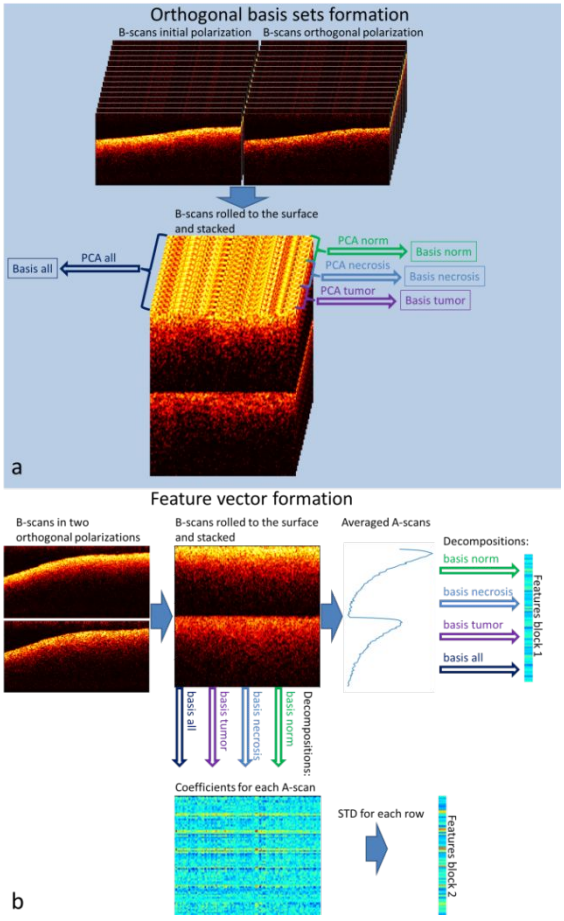

phys. stat. sol. (a) 201, No. 13 (2004) / www.pss-rapid.com R4

Figure 1 Figure 1 Schematic representation of the data processing. Panel **a** – formation of sets of basis vectors from the training dataset. Note that the diagnostically non-valued tissues were split into two categories "norm" data (white and grey matter) and "necrosis"; the "tumor tissue" data was split into three diagnostically valued categories (astrocytomas and gliomas of different grades). Panel **b** – feature vector formation from the pair of B-scans in two orthogonal polarizations from the validation dataset.

3. Results and discussion

Examples of OCT images from the dataset as well as the corresponding histology images are presented in figure 2.

Visual assessment of the CP OCT images shows that only the white matter images can be easily distinguished from the images of other types of brain tissue because of their high scattering that results in high-intensity images. This difference is especially profound in the cross-polarization channel. The features of scattering from the other types of tissue are much closer to each other and for the pathological tissues (tumorous and necrotic) can fluctuate across a wide range, making it more difficult for the user to distinguish between them. The characteristic feature of the tumorous tissue as described previously [31] is the scattering variability across the B-scan, which can be seen as the variability in the penetration depths, or as inclusions in the bulk of the tissue, however, this feature is not always clearly visible in the images of tumorous tissue. Another characteristic of tumorous tissue is its generally lower scattering in cross-polarization, which could be explained by the lack of structure in such tumorous tissue, however, this characteristic is also subtle in some cases and requires a significant level of experience of the user.

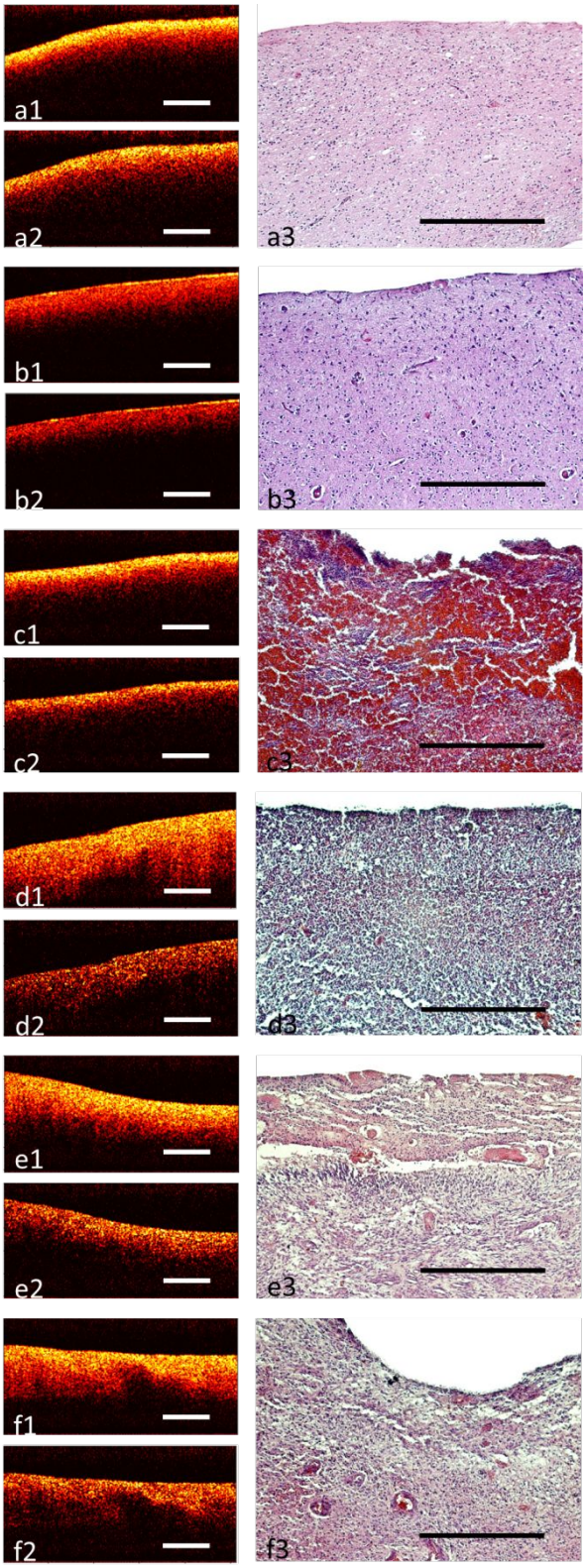

Figure 2 a - Examples of the images of 6 different types of brain tissue used in the study in co- (image 1 in each panel) and cross- (image 2 in each panel) polarizations, as well as the corresponding histology (image 3 in each panel). Panel **a**

– white matter, panel **b** – cortex, panel **c** – necrosis (all non-tumorous, diagnostically non-valued tissues); panel **d** – tumor Grade II, panel **e** – tumor grade IV with necrosis, panel **f** – tumor grade IV without necrosis (all tumorous, diagnostically valued tissues). Each scale bar represents 0.5 mm.

Therefore, in some cases the CP OCT signals of diagnostically valued and of non-valued tissue samples are similar: grey matter vs. tumor tissue without necrosis; white matter and necrosis vs. tumor tissue with necrotic areas. In these cases, visual assessment could be difficult and lead to misclassification which would reduce its value for biopsy guidance.

The limitation of visual assessment is its subjectivity, so the accuracy of such an assessment depends on the skills of the neurosurgeon in the practical application of these criteria. It is therefore necessary to make the qualitative evaluation of CP OCT signal more objective. The aim of this study was to improve the visual assessment of cross-section CP OCT images (B-scans) by applying machine learning algorithms.

In the case of the algorithm for stereotactic biopsy a "positive" outcome of the algorithm corresponds to the detection of tumorous tissue. In this case, the algorithm parameters should be adjusted to minimize the number of false-positive evaluations even at the cost of an increasing number of false-negative evaluations, since false positives will lead to the acquisition of diagnostically non-valued samples, while false negative will lead to a further search for a better site for the biopsy.

The performance of the proposed algorithm was accessed using the area under the receiver-operation characteristic curve (ROC-curve) value and was equal to 0.93. As seen from figure 3, the value of the threshold that provides the highest diagnostic accuracy (DA = 0.85) corresponds to a false positive range (FPR) equal to 0.26, which is almost equal to the FPR of current stereotactic biopsy guidance methods. However by appropriate threshold choice the FPR can be reduced with the sacrifice of true positive rate (TPR) and DA. E.g. FPR < 0.05 can be achieved with a TPR ~ 0.72 and DA ~ 0.8, while FPR < 0.01 can be achieved with a TPR ~ 0.45 and DA ~ 0.66. These values are more suitable for biopsy guidance since, in this scenario, the cost of the false-positive evaluation is much higher than that of a false-negative as it leads to a second surgical intervention.

Several limitations of the study, which should be overcome in future work must be outlined. Firstly, the study was performed on *ex vivo* samples, thus the effect of vessels and shadow artifacts from such vessels on the performance of the algorithm is unknown. It is obvious, that the presence of vessels will affect both the average A-scans and the variability of the A-scans. The most straightforward way to overcome this influence is to exclude A-scans with vessels from the analysis, but the effectiveness of such processing would need to be investigated. In addition, it should be noted that the detection of vessels is a separate, important task, which can be accomplished with OCT assistance, since damaging the vessels and causing hemorrhage is one of the main risks of stereotactic biopsy.

Secondly, the study was performed on a limited number of patients, thus the current algorithm may not account for all the individual features of brain tissue from patient to patient, does not span all the potential variability of tumorous tissues, does not include tumorous tissue of some etiologies (e.g. metastasis from other tumors), and does not include the grey matter of the basal ganglia, which may differ in its optical properties and appearance in OCT images from the grey matter of the cortex. The addition of all the aforementioned tissue types will affect the overall algorithm performance results. However, the current small sample study shows the potential of the approach, while the aforementioned drawback should be overcome with the collection of more samples from a greater number of patients, thus making the algorithm more reliable.

Thirdly, an OCT device used for stereotactic biopsy guidance should have a scanner compatible with standard biopsy equipment such as a biopsy needle, so that it is possible to operate in the canal used for the biopsy. Such a device is under development in our laboratory. The performance of the classification algorithm will be tested for images from the new device since it could be sensitive to some individual parameters such as the device point spread function. However, we believe that even if the algorithm performance may decrease, the developed approach allows it to be adapted to the parameters of particular devices.

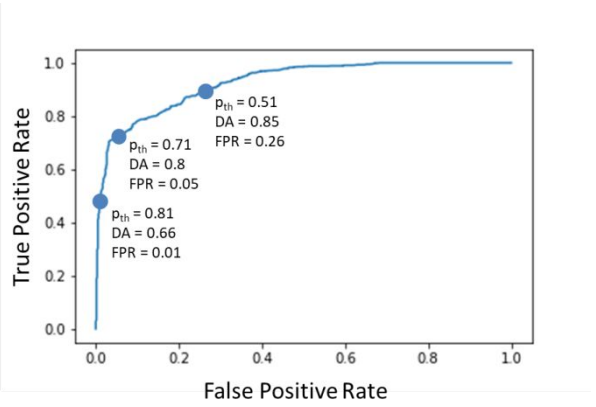

Figure 3 ROC-curve for classification to distinguish between tumorous and non-tumorous tissues for biopsy guidance, with tumorous tissue being represented by positive results. The dots on the curve represent

possible choices of the threshold value of the algorithm output (p_{th}) and the corresponding diagnostic accuracy (DA) and false positive rate (FPR) values.

4. Conclusion

A method for classification to distinguish between tumorous and non-tumorous brain tissues, based on quantitative analysis of CP OCT images has been proposed. This approach is a promising way for brain tumor stereotactic biopsy guiding using OCT. Due to the possibility of generating low false-positive rates in determining tumorous from non-tumorous tissue, the use of the proposed method can decrease the number of diagnostically non-valued samples and minimize the risk of causing unnecessary bleeding. This approach also could be extended to different clinical tasks, such as surgical guidance during malignant brain tumor resection.

Acknowledgements The brain tissue OCT images dataset collection and the development of the method for brain tissue classification were supported by Russian Foundation for Basic Research Russian Foundation for Basic Research, grant No 18-29-01049 (AAM, EBK, KSYa, NDG). The OCT device development was supported by the State Task of IAP RAS No 0035-2019-0013 (AAM, GVG).

References

1. Kohler, B.A., et al., *Kohler, B. A. Annual report to the nation on the status of cancer, 1975-2007, featuring tumors of the brain and other nervous system.* J Natl Cancer Inst, 2011. **103**(9): p. 714-36.
2. Ostrom, Q.T., et al., *Ostrom, Q. T. CBTRUS statistical report: Primary brain and central nervous system tumors diagnosed in the United States in 2006-2010.* Neuro Oncol, 2013. **15 Suppl 2**: p. ii1-56.
3. Ostrom, Q.T., et al., *The epidemiology of glioma in adults: a "state of the science" review.* Neuro Oncol, 2014. **16**(7): p. 896-913.
4. Ho, V.K., et al., *Changing incidence and improved survival of gliomas.* Eur J Cancer, 2014. **50**(13): p. 2309-18.
5. Zhao, S., et al., *Intraoperative fluorescence-guided resection of high-grade malignant gliomas using 5-aminolevulinic acid-induced porphyrins: a systematic review and meta-analysis of prospective studies.* PLoS One, 2013. **8**(5): p. e63682.
6. Eljamel, S., *5-ALA Fluorescence Image Guided Resection of Glioblastoma Multiforme: A Meta-Analysis of the Literature.* Int J Mol Sci, 2015. **16**(5): p. 10443-56.
7. Kubben, P.L., et al., *Intraoperative MRI-guided resection of glioblastoma multiforme: a systematic review.* Lancet Oncol, 2011. **12**(11): p. 1062-70.
8. Suero Molina, E., S. Schipmann, and W. Stummer, *Maximizing safe resections: the roles of 5-aminolevulinic acid and intraoperative MR imaging in glioma surgery-review of the literature.* Neurosurg Rev, 2017.
9. Potapov, A.A., et al., *[Clinical guidelines for the use of intraoperative fluorescence diagnosis in brain tumor surgery].* Zh Vopr Neirokhir Im N N Burdenko, 2015. **79**(5): p. 91-101.
10. Stummer, W., et al., *Extent of Resection and Survival in Glioblastoma Multiforme.* Neurosurgery, 2008. **62**(3): p. 564-576.
11. McGirt, M.J., et al., *Independent association of extent of resection with survival in patients with malignant brain astrocytoma.* Journal of Neurosurgery, 2009. **110**(1): p. 156-162.
12. Colditz, M.J. and R.L. Jeffree, *Aminolevulinic acid (ALA)–protoporphyrin IX fluorescence guided tumour resection. Part 1: Clinical, radiological and pathological studies.* Journal of Clinical Neuroscience, 2012. **19**(11): p. 1471-1474.
13. Zoeller, G.K., et al., *Outcomes and management strategies after nondiagnostic stereotactic biopsies of brain lesions.* Stereotact Funct Neurosurg, 2009. **87**(3): p. 174-81.
14. Dammers, R., et al., *Safety and efficacy of frameless and frame-based intracranial biopsy techniques.* Acta Neurochir (Wien), 2008. **150**(1): p. 23-9.
15. Dammers, R., et al., *Towards improving the safety and diagnostic yield of stereotactic biopsy in a single centre.* Acta Neurochir (Wien), 2010. **152**(11): p. 1915-21.
16. Tilgner, J., et al., *Validation of intraoperative diagnoses using smear preparations from stereotactic brain biopsies: intraoperative versus final diagnosis--influence of clinical factors.* Neurosurgery, 2005. **56**(2): p. 257-65; discussion 257-65.
17. Woodworth, G., et al., *Accuracy of frameless and frame-based image-guided stereotactic*

brain biopsy in the diagnosis of glioma: comparison of biopsy and open resection specimen. Neurol Res, 2005. **27**(4): p. 358-62.

18. Heper, A.O., et al., *An analysis of stereotactic biopsy of brain tumors and nonneoplastic lesions: a prospective clinicopathologic study.* Surg Neurol, 2005. **64 Suppl 2**: p. S82-8.
19. Gralla, J., et al., *Frameless stereotactic brain biopsy procedures using the Stealth Station: indications, accuracy and results.* Zentralbl Neurochir, 2003. **64**(4): p. 166-70.
20. Shooman, D., A. Belli, and P.L. Grundy, *Image-guided frameless stereotactic biopsy without intraoperative neuropathological examination.* J Neurosurg, 2010. **113**(2): p. 170-8.
21. Grossman, R., et al., *Haemorrhagic complications and the incidence of asymptomatic bleeding associated with stereotactic brain biopsies.* Acta Neurochir (Wien), 2005. **147**(6): p. 627-31; discussion 631.
22. Field, M., et al., *Comprehensive assessment of hemorrhage risks and outcomes after stereotactic brain biopsy.* J Neurosurg, 2001. **94**(4): p. 545-51.
23. Dorward, N.L., et al., *The advantages of frameless stereotactic biopsy over frame-based biopsy.* Br J Neurosurg, 2002. **16**(2): p. 110-8.
24. Lunsford, L.D., et al., *Establishing a benchmark for complications using frame-based stereotactic surgery.* Stereotact Funct Neurosurg, 2008. **86**(5): p. 278-87.
25. Osman, H., et al., *In Vivo Microscopy in Neurosurgical Oncology.* World Neurosurg, 2018.
26. Vasefi, F., et al., *Vasefi, F. Review of the potential of optical technologies for cancer diagnosis in neurosurgery: a step toward intraoperative neurophotonics.* Neurophotonics, 2016. **4**(1): p. 011010.
27. Vasefi, F., et al., *Review of the potential of optical technologies for cancer diagnosis in neurosurgery: a step toward intraoperative neurophotonics.* Neurophotonics, 2017. **4**(1): p. 011010.
28. Yashin, K.S., et al., *[Optical coherence tomography in neurosurgery].* Zh Vopr Neirokhir Im N N Burdenko, 2017. **81**(3): p. 107-115.
29. Huang, D., et al., *Optical coherence tomography.* Science, 1991. **254**(5035): p. 1178-1181.
30. Bohringer, H.J., et al., *Bohringer, H. J. Imaging of human brain tumor tissue by near-infrared laser coherence tomography.* Acta Neurochir (Wien), 2009. **151**(5): p. 507-17; discussion 517.
31. Yashin, K., et al., *Visual assessment criteria of microstructural ex vivo co-and cross-polarized optical coherence tomography images in gliomas.* Proceedings of SPIE Vol. 10685 (SPIE, Bellingham, WA 2018), 106853F, 2018.
32. Kut, C., et al., *Kut, C. Detection of human brain cancer infiltration ex vivo and in vivo using quantitative optical coherence tomography.* Science Translational Medicine, 2015. **7**(292): p. 292ra100-292ra100.
33. Yuan, W., et al., *Robust and fast characterization of OCT-based optical attenuation using a novel frequency-domain algorithm for brain cancer detection.* Scientific reports, 2017. **7**: p. 44909.
34. Böhringer, H.J., et al., *Imaging of human brain tumor tissue by near-infrared laser coherence tomography.* Acta Neurochirurgica, 2009. **151**(5): p. 507-517.
35. Sun, C., et al. *Neurosurgical hand-held optical coherence tomography (OCT) forward-viewing probe*. in *SPIE BiOS*. 2012. SPIE.
36. Lankenau, E., et al., *Combining Optical Coherence Tomography (OCT) with an Operating Microscope.* 2007. **114**: p. 343-348.
37. El-Haddad, M.T. and Y.K. Tao, *Advances in intraoperative optical coherence tomography for surgical guidance.* Current Opinion in Biomedical Engineering, 2017. **3**: p. 37-48.
38. Gubarkova, E.V., et al., *Multi-modal optical imaging characterization of atherosclerotic plaques.* Journal of Biophotonics, 2016. **9**(10): p. 1009-1020.
39. Gladkova, N., et al., *Evaluation of oral mucosa collagen condition with cross-polarization optical coherence tomography.* Journal of Biophotonics, 2013. **6**(4): p. 321-329.
40. Wang, H., et al., *Polarization sensitive optical coherence microscopy for brain imaging.* Optics Letters, 2016. **41**(10): p. 2213.
41. Boas, D.A., et al., *Polarization-sensitive optical coherence tomography of the human brain connectome.* SPIE Newsroom, 2017.
42. Gladkova, N., et al., *Cross-polarization optical coherence tomography for early bladder-cancer detection: statistical study.* Journal of biophotonics, 2011. **4**(7-8): p. 519-532.

Graphical Abstract for Table of Contents

Text: The study aimed to create a machine learning method for differentiating diagnostically valued tumorous tissue from diagnostically "non-valued" non-tumorous tissues in the human brain, using cross-polarization optical coherence tomography (CP OCT) in order to provide guidance for stereotactic biopsies. A method of feature extraction from OCT data in two orthogonal polarization channels has been proposed and a classification algorithm for the resulting feature vectors has been created. If used for stereotactic biopsy guidance, the proposed approach could decrease the number of excised diagnostically non-valued samples and minimize the invasiveness of the procedure and the risk of excessive bleeding

Image:.